Journal of Engineering Science and Technology
Vol. 12, No. 1 (2017) 265 - 279
© School of Engineering, Taylor's University

# HEAT TRANSFER ENHANCEMENT USING ALUMINA NANOFLUID IN CIRCULAR MICRO CHANNEL

K. S. ARJUN*, K. RAKESH

Department of Mechanical Engineering, Indian Institute of Technology (ISM), Dhanbad-826004, India
*Corresponding Author: arjun@mece.ism.ac.in

**Abstract**

In this study, thermal and flow behavior models for circular microchannel using water and its nanofluids with alumina as a coolant fluid in single phase flow have been developed. A finite volume-based CFD technique is used and models are solved by using Fluent Solver. The 2D axis symmetric geometry with structured mesh and 100 x 18 nodes are used for single phase flow with $Al_2O_3$ nanoparticles of 23 nm average diameter. Viscous laminar and standard k-ε models are used to predict the steady temperature in laminar and turbulent zone. The heat transfer enhancement upto 83% in laminar and turbulent zones are obtained with the Re ranging from 5 to 11980 and particle volume concentration from 0 to 5%. Even though the pressure drop increases with increase in Re, it is comparatively less compared to the corresponding decrease in temperature. The increase in temperature depends on Re and Pe; but the temperature distribution is found to be independent of radial position even for very low Pe. Comparison with analytical results both in laminar and turbulent zone is provided to justify the assumptions introduced in the models and very close agreement is observed statistically. Nusselt number can well predict the analytical data.

Keywords: Circular microchannels, Nanofluids, Computational fluid dynamics, Heat transfer coefficient, Pressure drop.

## 1. Introduction

In recent years the research in the field of single- and two-phase flow heat transfer at a micro scale level has been constantly increasing due to the rapid growth of the technology applications that require the transfer of high heat rates in a relatively small space and volume. Such applications span from compact heat exchangers to cooling systems for computer CPU to microfluidic devices. The

**Nomenclatures**

| | |
|---|---|
| $C_p$ | Specific heat, kJ/kg K |
| $D$ | Diameter, Dimensional, m |
| $F$ | External body force, N |
| $h$ | Heat transfer coefficient, W/m$^2$K |
| $k$ | Thermal conductivity, W/mK |
| $L$ | Length, m |
| $m$ | Mass, kg |
| Nu | Nusselt number |
| $p$ | Pressure, kPa |
| Pe | Peclet number |
| Pr | Prandtl number |
| Re | Reynolds number |
| $t$ | Time, s |
| $T$ | Temperature, °C |
| $T_{ref}$ | Reference temperature, 25°C |
| $u$ | Mean fluid velocity, m/s |
| $x$ | Axial distance, m |
| $y$ | Radial distance, m |

***Greek Symbols***

| | |
|---|---|
| $\bar{\bar{\tau}}$ | Stress tensor |
| $\mu$ | Volumetric concentration, molecular/turbulent viscosity, kg/m.s |
| $\varepsilon$ | Rate of dissipation, J/kg.s |
| $\nu$ | Kinematic viscosity, m$^2$/s |
| $\rho$ | Density, kg/m$^3$ |
| $\phi$ | Volume concentration |

**Subscripts**

| | |
|---|---|
| $f$ | Fluid |
| $in$ | Channel inlet |
| $nf$ | Nanofluid |
| $out$ | Channel outlet |
| $r$ | Radial |

conductivity of the suspended nanoparticles in a conventional fluid is found greater than conventional fluid motivates many researchers of their application in Heat exchanger. The large surface area of nanoparticles allows for more heat transfer. Another advantage is the mobility of the particles, attribute to the tiny size, which may bring about micro-convection of fluid and increased heat transfer. Because of the small particles, they weigh less and the chances of sedimentation are also less. This will make the nanofluids more stable. Large enhancement of conductivity was achieved with a very small concentration of particles that completely maintained the Newtonian behaviour of the fluid. The rise in viscosity was nominal; hence, pressure drop as increased only marginally. Unlike the situation with micro- slurries, the enhancement of conductivity was found to depend not only on particle concentration but also on particle size. In general, with decreasing particle size, an increase in enhancement was observed [1-5].

Very good and updated reviews of these aspects are given [6-7]. Scaling effects which play a relevant role in micro scale single-phase flow heat transfer are viscous heating, thermal entrance length and axial conduction (conjugate heat transfer). The most recent works, where scaling effects above described in detail are properly accounted for, have shown how micro scale heat transfer in liquid single-phase flow, both for laminar and turbulent flow, can be well predicted using what is known from the knowledge of heat transfer in macro scale, i.e., Nu = 4.36 for laminar flow and a correlation [8] for turbulent flow. With 1–5 volume % nanoparticles concentrations, the thermal conductivity of the suspensions can increase more than 20% [9]. 40% heat transfer enhancement was found with $Al_2O_3$ particles [10]. The heat transfer enhancement increases with particle volume concentration [11]. Convective heat transfer coefficient for nanofluids with a volume fraction of 0.03 was found to be 12% lower than that of pure water [12]. But, opposite conclusions have also been reported [9, 13-14].

An extensive study on fluid flow and heat transfer in the microchannel heat transfer was proposed by Tuckerman and Pease [15]. Besides, turbulent convection in microchannels is believed as an effective cooling mechanism for high power density systems [16, 17]. Besides, [18] and [19] stated that microchannel provides a very high surface area to volume ratio, small coolant requirement, large heat transfer coefficient, as well as very small mass and volume per heat load. It is numerically confirmed that the nanofluids can bring heat transfer enhancement by increasing the volume of concentration [20].

The experimental study of microchannel heat sink performance using CuO-$H_2O$ in the range of volume fraction between 0.2 and 0.4% indicated that the nanofluids could absorb more heat and attained lower wall temperatures than pure liquid [21]. There was also a slight effect in the increase in pressure drop compared to pure liquid cooled. About 32% of increase of heat transfer coefficient of $Al_2O_3$ at a diameter of 170 nm compared to distilled water at 1.8% of volume fraction in laminar regime was obtained [22]. They also discovered an increment in the Nusselt numbers with the increase in Reynold numbers. Meanwhile, Lee and Mudawar [23] experimentally conducted the effectiveness of $Al_2O_3$-water for single-phase and two-phase heat transfer. For single-phase, heat transfer coefficient was increased because of the high thermal conductivity of nanofluids. The enhancement was quite weak in the fully developed region because of the effect of thermal boundary layer development. Besides, they found that the two-phase cannot be applied to microchannel because of catastrophic failure.

The results displayed an increase in Reynolds number and volume concentrations, as well as an increase in the Nusselt number, with the variation pressure saw dropped for inlet, whereas an increase in the outlet section [24]. A heat removal rate of $0.79\times10^4$ kW/m$^2$ with single phase flow was demonstrated [25]. Computer chips currently require cooling rates up to approximately $1\times10^4$ kW/m$^2$ [26], meaning new solutions need to be found for the next generation of devices that maximize heat transfer rates with minimal pressure drops. Microchannels, with their large heat transfer surface to volume ratio, cooled with gas or liquid coolant, have shown some potential to provide adequate cooling necessary to maintain temperature values low enough for the electronic components to operate [27]. The experimental results of pressure drop and heat transfer confirm that including the entrance effects, the conventional theory is

applicable for water flow through micro-channels [28]. Heat transfer in microchannels can be described by standard theory and correlations, but scaling effects (entrance effects, conjugate heat transfer, viscous heating, electric double layer effects, temperature dependent properties, surface roughness, rarefaction and compressibility effects), often negligible in macro-channels, have significant influence [29].

The heat transfer performance of silicon microchannels improved when nanofluids were used as coolants [30]. Enhancement of connective heat transfer was observed when the $Al_2O_3$ nanofluids were used through a copper tube and proposed that nanoparticle migration and the resulting boundary layer disturbance were the main reasons for the enhancement [31]. Microchannel performance could be improved by using fluids having high Prandtl numbers, high volume concentrations of nanoparticles and microchannels with high aspect ratios [32]. Carbon nanotube-$H_2O$ and Cu-$H_2O$ nanofluid in a microchannel reduced the temperature difference between the bulk nanofluid and bottom-heated wall [33]. Numerical investigation of water–diamond nanofluid cooled microchannel enhanced the performance by about 11% compared with pure water [34]. The nanofluid measurably enhanced the thermal performance of microchannel flow with the expense of more pumping power [35]. The heat transfer coefficient increased with the nanofluids particle concentration and Peclet number [36] in a circular tube under constant surface temperature. The heat transfer performance of water-based nanofluids can be increased in a microchannel heat sink having a steel substrate [37, 38].

The importance of nanofluids in electronics cooling is increasing due to miniaturization and safe working [39]. There is limited research related to performance study of microchannel heat exchangers using Computational Fluid Dynamics models. The strength of numerical simulations is the possibility to investigate small details that are impossible to observe in experiments. Computational Fluid Dynamics modeling and simulation of single phase circular micro channel flow and conjugate heat transfer were not studied at wide range of Re. In this work, Nusselt number and pressure drop of water based nanofluids of $Al_2O_3$ with 23 nm average diameter have been characterized in a circular microchannel of 0.1 m length and diameter of 0.5 mm. Water base nanofluid properties with different concentration of alumina nanoparticles [40] at 30$^o$C temperature and 100 kPa pressure are used in this investigation. The simulations have been performed for different nanoparticle volume concentrations (0-5%) and flow rates (5< Re <11980). The nanofluid temperatures have also been specifically analyzed and discussed.

## 2. Specification of Problem, Simulation and Validation

The geometry of circular micro channel and structured mesh is shown in Figs. 1 and 2. Based on $Re = Du\rho/\mu$, either viscous laminar model at Re < 2000 or standard k-ε model at Re > 2000 is used for laminar and turbulent flow.

The specified solver in Fluent uses a pressure correction based iterative SIMPLE algorithm with 1$^{st}$ order upwind scheme for discretizing the convective transport terms. A no slip boundary condition for non-porous wall surfaces and 2 D axis symmetry at centerline were assigned.

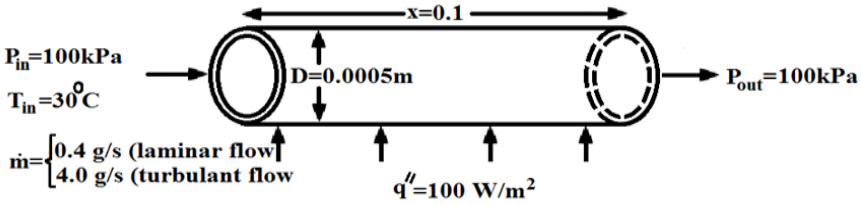


**Fig. 1. Fluid flow through a circular micro channel.**

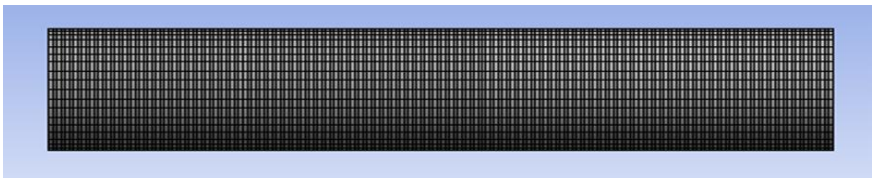

**Fig. 2. Geometry with structured mesh.**

The equation for conservation of mass, or continuity equation, can be written as follows:

$$\frac{\partial \rho}{\partial t} + \nabla \cdot (\rho \vec{v}) = S_m \tag{1}$$

Equation (1) is the general form of the mass conservation equation, and is valid for both incompressible compressible flows. The source $S_m$ is the mass added to the continuous phase from the dispersed second phase (e.g., due to vaporization of liquid droplets) and any user defined sources.

Conservation of momentum in an inertial (non-accelerating) reference frame is described by

$$\frac{\partial}{\partial t}(\rho \vec{v}) + \nabla \cdot (\rho \vec{v}\vec{v}) = -\nabla p + \nabla \cdot (\bar{\bar{\tau}}) + \rho \vec{g} + \vec{F} \tag{2}$$

where $p$ is the static pressure, $\bar{\bar{\tau}}$ is the stress tensor (described below), and $\rho \vec{g}$ and $\vec{F}$ are the gravitational body force and external body forces (e.g., that arise from interaction with the dispersed phase), respectively. $\vec{F}$ also contains other model dependent source terms such as porous-media and user-defined sources.

The stress tensor $\bar{\bar{\tau}}$ is given by

$$\bar{\bar{\tau}} = \mu \left( (\nabla \vec{v} + \nabla \vec{v}^T) - \frac{2}{3} \cdot \vec{v} I \right) \tag{3}$$

where $\mu$ is the molecular viscosity, $I$ is the unit tensor, and the second term on the right hand side is the effect of volume dilation.

ANSYS FLUENT solves the energy equation in the following form:

$$\frac{\partial}{\partial t}(\rho E) + \nabla \cdot \left(\vec{v}(\rho E + p)\right) = \nabla \cdot \left( K_{eff} \nabla T - \sum_j h_j \vec{J_j} + \left(\bar{\bar{\tau}}_{eff} \cdot \vec{v}\right)\right) + S_h \tag{4}$$

where $K_{eff}$ is the effective conductivity ($K + K_t$, where $K_t$ is the turbulent thermal conductivity, defined according to the turbulence model being used), and $\vec{J_j}$ is the

diffusion flux of species $j$. The first three terms on the right-hand side of Equation represent energy transfer due to conduction, species diffusion, and viscous dissipation, respectively. $S_h$ includes the heat of chemical reaction, and any other volumetric heat sources.

$$E = h - \frac{p}{\rho} + \frac{v^2}{2} \tag{5}$$

where sensible enthalpy $h$ is defined as

$$h = \sum_j Y_j h_j \tag{6}$$

$Y_j$ is the mass fraction of species $j$.

$$h_j = \int_{T_{ref}}^{T} c_{p,j} dT \tag{7}$$

$T_{ref}$ is used as 298.15 K.

As fluid flows through in a pipe at both hydraulic and thermally fully developed condition, the Nusselt number is constant for laminar flow and it follows the Dittius-Boelter equation for turbulent flow.

$$\frac{hD}{k} = 4.36 \Rightarrow h \approx K \text{ for laminar flow} \tag{8}$$

$$\frac{hD}{k} = 0.023 \left(\frac{Dv\rho}{\mu}\right)^{0.8} \left(\frac{C_p \mu}{k}\right)^{0.4} \Rightarrow h \approx K^{0.6} v^{0.8} \mu^{-0.4} \quad \text{for turbulent flow} \tag{9}$$

From Eq. 8 and Eq. 9, it is clear that thermal conductivity has greater effect on heat transfer coefficient for laminar flow as compared to turbulent flow. This implies the enhancement effect due to the increased thermal conductivity of nanofluids is significantly weaker for turbulent flow than for laminar. The enhancement in turbulent flow is also dependent on flow rate in addition to viscosity and specific heat. Since $h \approx K^{0.6}\ \mu^{-0.4}\ C_p^{0.4}$ and because increased nanoparticle concentration enhances viscosity and degrades specific heat, the enhancement effect of nanoparticles in turbulent flow is further reduced compared to thermal conductivity alone.

For 2D axis symmetric geometries, the continuity equation is given by

$$\frac{\partial p}{\partial t} + \frac{\partial}{\partial x}(\rho v_x) + \frac{\partial}{\partial r}(\rho v_r) + \frac{p v_r}{r} = 0 \tag{10}$$

where $x$ represents axial coordinate in the direction of flow, $r$ is the radial coordinate i.e. transverse direction, $v_x$ is the axial velocity, and $v_r$ is the radial velocity components. For 2D axis symmetric geometries, the axial and radial momentum conservation equations are given by

$$\frac{\partial}{\partial t}(\rho v_x) + \frac{1}{r}\frac{\partial}{\partial x}(r\rho v_x v_x) + \frac{1}{r}\frac{\partial}{\partial r}(r\rho v_r v_x) = \frac{-\partial p}{\partial x} + \frac{1}{r}\frac{\partial}{\partial x}\left[r\mu\left(2\frac{\partial v_x}{\partial x} - \frac{2}{3}(\nabla \cdot \vec{v})\right)\right] + \frac{1}{r}\frac{\partial}{\partial r}\left[r\mu\left(\frac{\partial v_x}{\partial r} + \frac{\partial v_r}{\partial v_x}\right)\right] + F_x$$

and

$$\frac{\partial}{\partial t}(\rho v_r) + \frac{1}{r}\frac{\partial}{\partial x}(r v_x v_r) + \frac{1}{r}\frac{\partial}{\partial r}(r v_r v_r) \tag{11}$$

$$= \frac{-\partial \rho}{\partial r} + \frac{1}{r}\frac{\partial}{\partial x}\left[r\mu\left(\frac{\partial v_r}{\partial x} + \frac{\partial v_x}{\partial r}\right)\right] \tag{12}$$

$$+\frac{1}{r}\frac{\partial}{\partial r}\left[r\mu\left(2\frac{\partial v_r}{\partial r} - \frac{2}{3}(\nabla \cdot \vec{v})\right)\right] - 2\mu\frac{v_r}{r^2}$$

$$+\frac{2}{3}\frac{\mu}{r}(\nabla \cdot \vec{v}) + \rho\frac{v_r^2}{r} + F_r$$

where

$$\nabla \cdot \vec{v} = \frac{\partial v_x}{\partial x} + \frac{\partial v_r}{\partial r} + \frac{v_r}{r} \tag{13}$$

Since the microchannel with small radial thickness is horizontally placed, the external body force $F$ is taken as zero.

The turbulence kinetic energy, $k$, and its rate of dissipation, $\varepsilon$, are obtained solving the following transport equations:

$$\frac{\partial}{\partial t}(\rho k) + \frac{\partial}{\partial x_i}(\rho k v_i)$$

$$= \frac{\partial}{\partial x_j}\left[\left(\mu + \frac{\mu_t}{\sigma_k}\right)\frac{\partial k}{\partial x_j}\right] + G_k + G_b - \rho\varepsilon - Y_M + S_k \tag{14}$$

and

$$\frac{\partial}{\partial t}(\rho\varepsilon) + \frac{\partial}{\partial x_i}(\rho\varepsilon v_i) = \frac{\partial}{\partial x_j}\left[\left(\mu + \frac{\mu_t}{\sigma_\varepsilon}\right)\frac{\partial \varepsilon}{\partial x_j}\right]$$

$$+C_{1\varepsilon}\frac{\varepsilon}{k}(G_k + C_{3\varepsilon}G_b) - C_{2\varepsilon}\rho\frac{\varepsilon^2}{k} + S_\varepsilon \tag{15}$$

In these equations, $G_k$ represents the generation of turbulence kinetic energy due to the mean velocity gradients. $G_b$ is the generation of turbulence kinetic energy due to buoyancy. $Y_M$ represents the contribution of the fluctuating dilatation in compressible turbulence to the overall dissipation rate. $C_1\varepsilon$, $C_2\varepsilon$ and $C_3\varepsilon$ are constants. $\sigma_k$ and $\sigma_\varepsilon$ are the turbulent Prandtl numbers for $k$ and $\varepsilon$ , respectively. $S_k$ and $S_\varepsilon$ are user-defined source terms.

The turbulent (or eddy) viscosity $\mu_t$ is computed by combining $k$ and $\varepsilon$ as follows:

$$\mu_t = \rho C_\mu \cdot \frac{k^2}{\varepsilon} \tag{16}$$

The model constant $C_1\varepsilon$, $C_2\varepsilon$, $C_\mu$, $\sigma_k$ and $\sigma_\varepsilon$ have the default values of 1.44, 1. 92, 2.1, 0.09, 1 and 1.3 respectively. $C_3\varepsilon$ has values 1 (along) or 0 (perpendicular) for flow direction with gravity. The governing equation for energy is same as represented in Eq. 4. The bulk mean temperature, $T_{m,x}$ and wall temperature, $T_{w,x}$ with distance $x$ from the microchannel entrance can be obtained by doing the thermal energy balance around the microchannel as shown in the following equations.

$$T_{m,x} = T_{in} + \frac{q''\pi D x}{m C_{p,nf}} \tag{17}$$

$$T_{w,x} = T_{m,x} + \frac{q''}{h} \tag{18}$$

where, $T_{in}$ (303.15 K), is the specified inlet temperature. $q''$ and $h$ are the heat flux and heat transfer coefficient respectively.

To characterize the effect of fluid flow on the thermal behaviour of the microchannel heat exchanger, Peclet number Pe is defined as

$$Pe = \frac{\rho_f C_{p,f} u}{(k/L)} \tag{19}$$

Three different mesh sizes with rectangular elements are applied in the grid test, to use wall y+ as the appropriate near-wall treatment (wall functions modeling as k-ε model is used). This is achieved by refining the mesh, with particular attention to the near-wall region so as to achieve the desired wall y+, i.e. the distance from the wall to the centroid of the wall-adjacent cells.

## 3. Results and Discussion

The solution is tested for 100 x 12 (Nu = 175.862) and 100 x 24 (Nu = 175.948) grid sizes and it was noted that decreasing the 100 x 18 (Nu = 175.949) does not result in any considerable difference in Nu for Re = 11980 and hence chosen as the optimal size. The different mesh configurations and corresponding wall y+ had a significant influence on the computed Nusselt number results. Mesh configurations of 100 x 18 in the x and y directions have wall y+ values resolved in the region, $7 < y+ < 8$ and ensured grid independence. Values close to $y+ \approx 8$ are found most desirable. Extensive validations of our flow solver are performed with available analytical solutions of [41] in terms of fully developed Nusselt numbers for water.

Nusselt numbers and pressure drop with nanofluid concentrations 0 to 5% at Re 5 to 50 and Re 1198 and 11980 are shown in Fig. 3 and 4 respectively. As Re and $\varphi$ increases, Nu and pressure drop increases. Variation of wall temperature were evident using Alumina/water nanofluid in circular micro channel for different values of Re. The effect of Re on the variation of nanofluid temperature with axial position showed that there is less variation in nanofluid temperature with axial distance at Re 5 and no change at still higher Re. The Pe increases with increase in Re and thus the contribution of convective heat flux dominates over conductive heat flux at higher Re and inlet temperature of fluid penetrates more towards the outlet at higher Pe.

The variation of nanofluid temperature with radial position at different values of x and at different values of Re shows that there is no variation of temperature in y direction as convective heat transfer rate dominates over conductive heat transfer rate even at Re = 5 for which also Pe >> 1. But at very low value of Re, the Pe is much less than 1, conductive heat transport dominates over convective heat transfer and variation of temperature of nanofluid is very high, but still there is no temperature distribution observed with radial position, as the diameter of the channel is very less compared to the length. A large axial temperature rise could be attributed with the decreased specific heat for the nanofluid compared to the base fluid with higher enhancement in the entrance region and weaker enhancement in the fully developed region with higher concentrations produced greater sensitivity to heat flux as reported earlier [40]. Temperature contour plots support profile differences towards exit as Re increases. This also show that there is no variation of temperature in the radial direction.

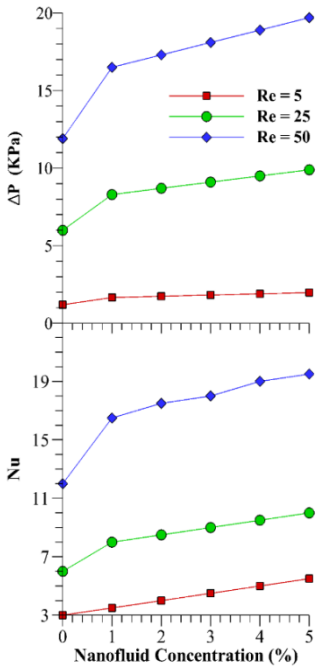


**Fig. 3. Nu and pressure drop at lower Re and nanofluid concentrations.**

The pressure drop of $Al_2O_3$-water nanofluids are approximately the same as those of water in the given conditions and implies that the nanofluid incurs no penalty of pump power and may be suitable for practical application. This observation is in accordance with the pumping power requirement of the Alumina/water nanofluid as nearly equal to that of water for the same Pe [42] and pressure loss increases only slightly with increase in volume concentration of nanofluids [43]. The entrance effect is much shorter in turbulent flow and negligible in present case since pipe length is much shorter than 10 diameters and further, its dependence on Re is weaker. The average ratio of friction factor of nanofluid to that of base fluid was 1.10 for 1% volume concentration. There is no friction, since the surface of the wall being smooth and as the Pr is higher than unity for water and nanofluids at all volume concentrations; velocity diffusivity dominates in comparison to thermal diffusivity. It is observed that as Re increases, pressure drop increases linearly with axial distance at all Re for all nanofluid volume concentrations. The low amounts of pressure drop in this study might be due to the fact that the flow was not simulated as two phase and not including effects such as Brownian motion etc. Even though axial velocity decrease with increase in nanofluid concentration for laminar and turbulent zones, no variation is found at a particular concentration except for the entrance length. Velocity profile is flat at very low Re and parabolic at higher Re.

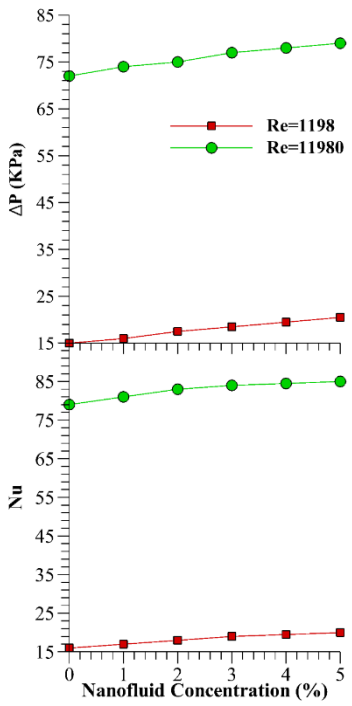


**Fig. 4. Nu and pressure drop at higher Re and nanofluid concentrations.**

In case of laminar flow, Nusselt number increases by 83% from 0 to 5% Alumina/water nanofluid and in turbulent flow, the increase was 8%, even though the Nusselt number values in turbulent flow are higher in magnitude than laminar values. These results were in agreement [44] and contradict [40]; the latter opined that heat transfer enhancement was negligible in turbulent Alumina/water nanofluid flow in circular microchannel. The present results are in agreement with the experimental results of significant increase of the overall heat transfer coefficient in a miniature heat sink by dispersion of $Al_2O_3$ nanoparticles in water, with the decrease of thermal resistance of heat sink [45]. Similar results by use of $SiO_2$-water nanofluid [46] and nanofluid-cooled miniature plate fin heat sink [47] were also reported. The Nusselt number values are found to be independent of axial position which means that circular micro channel is at fully thermal developed condition in both laminar and turbulent types of flows. In laminar flow Nu = 4.36 (i.e. h ≈ k). To prove it, the ratio of heat transfer coefficients of nanofluids to water at different values of Re is found equal to ratio of thermal conductivity of nanofluid to water. Analytical and computational Nusselt numbers for laminar and turbulent flow of 0 to 5% nanofluids are shown in Fig. 5 that proves CFD results well predicted analytical Nusselt numbers.

The value of Pe for both Re = 1198 and Re = 11980 are much greater than 1, and hence temperature at all the points on x axis becomes equal to inlet temperature. As Re decreases to low value of 5, the Pe value decreases substantially and also residence time of fluid in channel increases due to decrease in inlet velocity of fluid. A substantial change in temperature from inlet to outlet is observed at lower Re. It is

also noticed that the use of water results in higher wall temperature than its nanofluids, and wall temperature at a particular axial position decreases with increase in nanoparticle concentrations, which might be due to combined effect of density, viscosity and thermal conductivity. This method is highly acceptable since excellent agreement between the simulated and experimental data is obtained with a Mean Absolute Error of 0.008% for laminar and 0.048% for turbulent flows. The present simulated values and experimental results for laminar and turbulent flows using Sum of Squares Error showed 99.73 and 100% accuracy in predicting analytical values of heat transfer coefficient. A good regression analysis with $R^2$ 0.9998*** and 1*** for laminar and turbulent flows between simulated values and experimental results were also obtained.

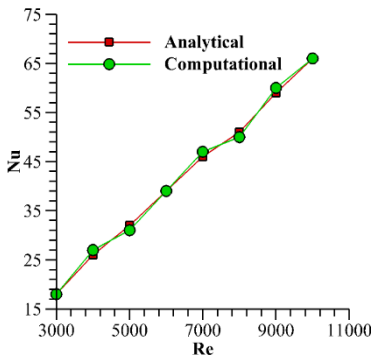


**Fig. 5. Validation of Nusselt numbers of water at different Re.**

## 4. Conclusions

In this study, the thermal and flow behaviour modelling of circular microchannel has been performed. Nusselt number and pressure drop have been formulated. The heat transfer during laminar and turbulent regime has been solved using the viscous laminar and standard k-ε methods. The predictions have been compared with reported analytical data. The results show that:

- Constant Nusselt numbers were achieved throughout the circular micro channel due to its hydrodynamically fully developed, but thermally developing conditions for a particular Re and nanofluid concentration with higher Nusselt numbers mostly in entrances region of micro channels. As the concentration of nanoparticle increases, Nusselt number also increases. With increase in Re, Nusselt numbers and pressure drop increases but wall and nanofluid temperatures decreases. Wall and nanofluid temperatures increase within the flow direction at very low Re, but has negligible variation at higher Re due to greater value of Pe.
- The enhancement of heat transfer in laminar nanofluid flow is greater as compared to turbulent nanofluid flow with respect to its base fluid. The nanofluid temperature is constant with respect to radial positions even at very low value of Pe. Velocity, pressure and temperature contours represent successfully the hydrodynamic and thermal behaviour of the microchannel system. The entrance length for fully developed flow depends on nanofluid

concentrations and Re. Even though axial velocity decrease with increase in nanofluid concentration for laminar and turbulent zones, no variation is found at a particular concentration except for the entrance length. Velocity profile is flat at very low Re and parabolic at higher Re. Wall temperature at an axial position decrease with respect to increase in nanofluid concentration. But there is no nanofluid temperature variation with radial position.

- Computed Nusselt numbers were found in close agreement with the analytical values statistically. At each Re, ratio of heat transfer coefficient of nanofluid to base fluid is found equal to ratio of thermal conductivity of nanofluid to base fluid.

## References

1. Hasan, M.I. (2011). Numerical investigation of counter flow microchannel heat exchanger with MEPCM suspension. *Applied Thermal Engineering*, 31, 1068-1075.
2. Peyghambarzadeh, S.M.; and Hashemabadi, S.H. (2011). Experimental study of heat transfer enhancement using water/ethylene glycol based nanofluids as a new coolant for car radiator. *International Communication in Heat and Mass Transfer*, 38, 1283-1290.
3. Das, S.K.; Choi, S.U.S.; and Patel, H.E. (2006). Heat transfer in nanofluids - A review. *Journal of Heat transfer engineering*, 27, 3-19.
4. Hung, T.C.; Yan, W.M.; Wang, X.D.; and Chang, C.Y. (2012a). Heat transfer enhancement in microchannel heat sinks using nanofluids. *International Journal of Heat and Mass Transfer*, 55, 2559–2570.
5. Hung, Y.H.; Ping, T.; and Teng, T.C. (2012b). Assessment of heat dissipation performance for nanofluid. *Applied Thermal Engineering*, 32, 132-140.
6. Morini, G.L. (2004). Single-phase convective heat transfer in microchannels: A review of experimental results. *International Journal of Thermal Sciences*, 43, 631-651.
7. Morini, G.L. (2006). Scaling effects for liquid flows in microchannels. *Heat Transfer Engineering*, 27, 64-73.
8. Gnielinski, V. (1976). New equations for heat and mass transfer in turbulent pipe and channel flow. *International Chemical Engineering*, 16, 359-368.
9. Lee, S.; Choi, S.S.; Li, S.A.; and Eastman, J.A. (1999). Measuring thermal conductivity of fluids containing oxide nanoparticles. *Journal of Heat Transfer*, 121(2), 280-289.
10. Heris, S.Z.; Etemad, S.G.; and Esfahany, M.N. (2006). Experimental investigation of oxide nanofluids laminar flow convective heat transfer. *International Communications in Heat and Mass Transfer*, 33(4), 529-535.
11. Bianco, V.; Chiacchio, F.; Manca, O.; and Nardini, S. (2009). Numerical investigation of nanofluids forced convection in circular tubes. *Applied Thermal Engineering*, 29(17), 3632-3642.
12. Pak, B.C.; and Cho, Y.I. (1999). Hydrodynamic and heat transfer study of dispersed fluids with submicron metallic oxide particles. *Experimental Heat Transfer an International Journal*, 11(2), 151-170.

13. Xuan, Y.; and Li, Q. (2003). Investigation on convective heat transfer and flow features of nanofluids. *Journal of Heat transfer,* 125(1), *151-155.*
14. Wen, D.; and Ding, Y. (2005). Experimental investigation into the pool boiling heat transfer of aqueous based γ-alumina nanofluids. *Journal of Nanoparticle Research,* 7(2-3), 265-274.
15. Tuckerman, D.B.; and Pease, R.F. (1981). High-performance heat sinking for VLSL. *IEEE Electronic Devices Letters*, 2, 126-129.
16. Azar, K. (2003). Cooling technologies option, part 1 and 2. Electronics. *Electronic Cooling*, 9 (3), 10-14 (Part 1); 9 (4), 30-36 (Part 2).
17. Ellsworth Jr., M.J.; and Simons, S. (2005). High powered chip cooling-air and beyond. *Electronic Cooling*, 3, 14-22.
18. Wu, H.Y.; and Cheng, P. (2003). Experimental study of convective heat transfer in silicon microchannel with different surface condition. *International Journal of Heat and Mass Transfer*, 46, 2537-2556.
19. Qu, W.; and Mudawar, I. (2002). Experimental and numerical study of pressure drop and heat transfer in a single-phase microchannel heat sink. *International Journal of Heat and Mass Transfer*, 45, 259-265.
20. Maiga, S.E.B.; Palm, S.J.; and Nguyen, C.T. (2005). Heat transfer enhancement by using nanofluids in forced convection flow. *International Journal of Heat and Fluid Flow*, 26, 530-546.
21. Chein, R.; and Chuang, J. (2006). Experimental microchannel heat sink performance studies using nanofluids. *International Journal of Thermal Sciences*, 46, 57-66.
22. Jung, Y.; Oh, H.S.; and Kwak, H.Y. (2009). Forced convective heat transfer of nanofluids in microchannels. *International Journal of Heat and Mass Transfer*, 52, 466-472.
23. Lee, J.; and Mudawar, I. (2007). Assessment of the effectiveness of nanofluids for single-phase and two-phase heat transfer in micro-channels. *International Journal of Heat and Mass Transfer*, 50, 452-463.
24. Sidik, N.A.C.; Yassin, M.M.; and Musa, M.N. (2015). Turbulent-forced convective heat transfer and pressure drop analysis of $Fe_3O_4$ magnetic nanofluid in a circular microchannel. *Jurnal Teknologi (Sciences & Engineering)*, 75, 11–15.
25. Asthana, A.; Zinovik, I.; Weinmueller, C.; and Poulikakos, D. (2011). Significant Nusselt number increase in microchannels with a segmented flow of two immiscible liquids: An experimental study. *International Journal of Heat and Mass Transfer*, 54 (7–8), 1456–1464.
26. Bar-Cohen, A.; Arik, M.; and Ohadi, M. (2006). Direct liquid cooling of high flux micro and nano electronic components. *Proceedings of the IEEE*, 94 (8), 1549–1570.
27. Tullius, J.F.; Vajta, R.; and Bayazitoglu, Y. (2011). A review of cooling in microchannels. *Heat Transfer Engineering*, 32 (7–8), 527–541.
28. Mishan, Y.; Mosyak, A.; Pogrebnyak, E.; and Hetsroni, G. (2007). Effect of developing flow and thermal regime on momentum and heat transfer in micro-scale heat sink. *International Journal of Heat and Mass Transfer*, 50, 3100–3114.

29. Rosa, P.; Karayiannis, T.G.; and Collins, M.W. (2009). Single-phase heat transfer in microchannels: The importance of scaling effects. *Applied Thermal Engineering*, 29 (17–18), 3447–3468.
30. Chein, R.; and Huang, G. (2005). Analysis of microchannel heat sink performance using nanofluids. *Applied Thermal Engineering*, 25, 3104–3114.
31. Wen, D.; and Ding, Y. (2004). Experimental investigation into convective heat transfer of nanofluids at the entrance region under laminar flow conditions. *International Journal of Heat and Mass Transfer*, 47, 5181–5188.
32. Koo, J.; and Kleinstreuer, C. (2005). Laminar nanofluid flow in micro heat-sinks. *International Journal of Heat and Mass Transfer*, 48 (13), 2652–2661.
33. Tsai, T.H.; and Chein, R. (2007). Performance analysis of nanofluid-cooled microchannel heat sinks. *International Journal of Heat Fluid Flow*, 28, 1013–1026.
34. Jang, S.P.; and Choi, S. (2006). Cooling performance of a microchannel heat sink with nanofluids. *Applied Thermal Engineering*, 26, 2457–2463.
35. Li, J.; and Kleinstreuer, C. (2008). Thermal performance of nanofluid flow in microchannels. *International Journal of Heat Fluid Flow*, 29, 1221–1232.
36. Fard, M.H.; Esfahany, M.N.; and Talaie, M.R. (2010). Numerical study of convective heat transfer of nanofluids in a circular tube two-phase model versus single-phase model. *International Communications in Heat and Mass Transfer*, 37, 91–97.
37. Mohammed, H.A.; Bhaskaran, G.; Shuaib, N.H.; and Abu-Mulaweh, H.I. (2011). Influence of nanofluids on parallel flow square microchannel heat exchanger performance. *International Communications in Heat and Mass Transfer*, 38, 1–9.
38. Mohammed, H.A., Gunnasegaran, P.; and Shuaib, N.H. (2011). Influence of various base nanofluids and substrate materials on heat transfer in trapezoidal microchannel heat sinks. *International Communications in Heat and Mass Transfer*, 38, 194–201.
39. Turgut, A.; and Elbasan, E. (2014). Nanofluids for electronics cooling. *2014 IEEE 20th International Symposium for Design and Technology of Electronics Packaging*, 23-26 Oct. 2014, Bucharest, Romania, 35-37.
40. Lee, J.; and Mudawar, I. (2007). Assessment of the effectiveness of nanofluids for single-phase and two-phase heat transfer in micro-channels. *International Journal of Heat and Mass Transfer*, 50(3), 452-463.
41. Gnielenski, V. (1976). New equations for heat and mass transfer in turbulent pipe and channels flow. *International Chemical Engineering*, 16, 359-368.
42. Raja, M.; Arunachalam, R.M.; and Suresh, S. (2012). Experimental studies on heat transfer of alumina/water nanofluid in a shell and tube heat exchanger with wire coil insert. *International Journal of Mechanical and Materials Engineering*, 7(1), 16-23.
43. Das, S.K.; Putra, N.; Thiesen, P.; and Roetzel, W. (2003). Temperature dependence of thermal conductivity enhancement for nanofluids. *Journal of Heat Transfer*, 125(4), 567-574.

44. Bianco, V.; Manca, O.; and Nardini, S. (2011). Numerical investigation on nanofluids turbulent convection heat transfer inside a circular tube. *International Journal of Thermal Sciences*, 50(3), 341-349.
45. Zirakzadeh, H.; Mashayekh, A.; Bidgoli, H.N.; and Ashjaee M. (2012). Experimental investigation of heat transfer in a novel heat sink by means of alumina nanofluids. *Heat Transfer Research*, 43 (8), 709-720.
46. Fazeli, S.A.; Hashemi, S.M.H.; Zirakzadeh, H.; and Ashjaee, M. (2012). Experimental and numerical investigation of heat transfer in a miniature heat sink utilizing silica nanofluid. *Superlattices and Microstructures*, 51(2), 247-264.
47. Hashemi, S.M.H.; Fazeli, S.A.; Zirakzadeh, H.; and Ashjaee, M. (2012). Study of heat transfer enhancement in a nanofluid-cooled miniature heat sink volume average technique. *International Communications in Heat and Mass Transfer*, 39 (6), 877-884.